

Supporting Information

Experimental Section

Characterization. The structures were characterized by scanning electron microscopy (SEM, Hitachi FE-SEM S-4800 operated at 1 KV), transmission electron microscopy (TEM, JEOL JEM-2100F operated at 200 KV), X-ray diffraction (Bruker AXS D8) and thermo-gravimetric analysis (Mettler Toledo). X-ray photoelectron spectroscopy was measured on an AXIS ULTRA DLD XPS System with MONO Al source (Shimadzu Corporation). Photoelectron spectrometer was recorded by using monochromatic Al KR radiation under vacuum at 5×10^{-9} Pa. All of the binding energies were referred to the C1s peak at 284.6 eV of the surface adventitious carbon. The electrochemical characterizations of the fiber-shaped supercapacitor were conducted on an electrochemical workstation (CHI 660D) and Arbin electrochemical station (MSTAT-5 V/10 mA/16Ch). The bending tests of the hybrid fiber and fiber-shaped supercapacitor were performed on a table-top universal testing instrument (HY-0350).

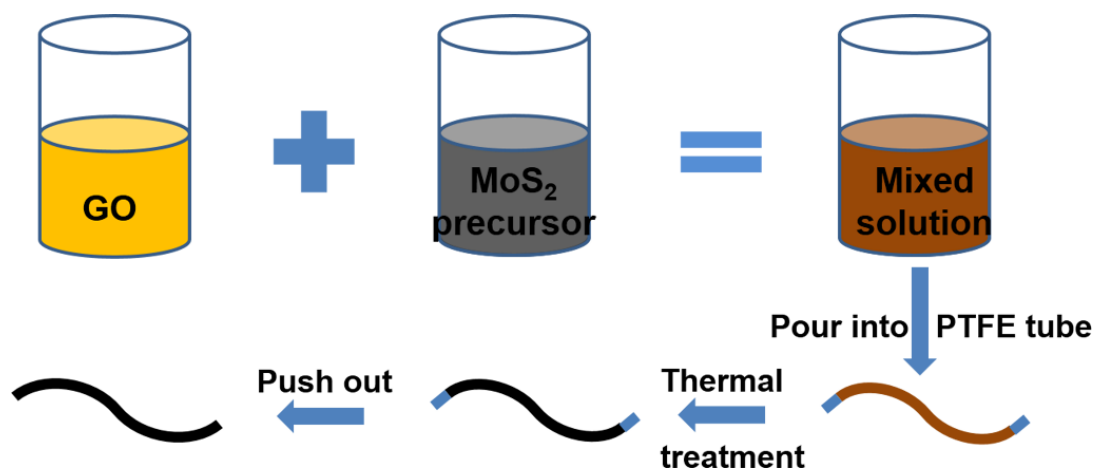


Figure S1. Schematic illustration to the synthesis of graphene/MoS₂ hybrid fiber.

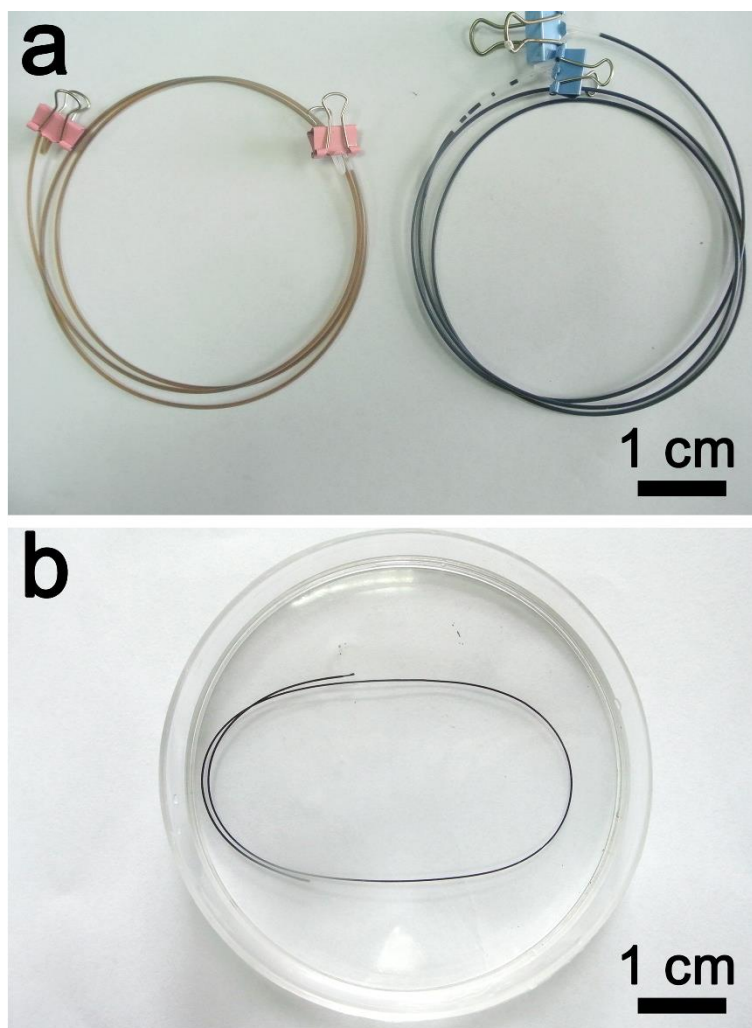


Figure S2. **a.** Photograph of polytetrafluoroethylene (PTFE) tubes filled with graphene oxide (GO) (left) and GO/(NH₄)₂MoS₄ (right) solutions. **b.** Photograph of the as-prepared graphene/MoS₂ hybrid fiber collected in water.

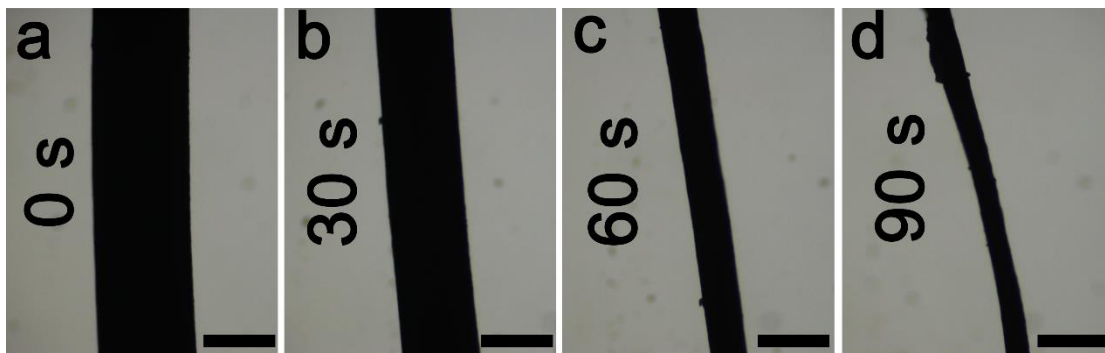


Figure S3. Micrographs of a wet graphene/MoS₂ hybrid fiber (released from PTFE tube) during drying in air. Scale bar, 300 μm .

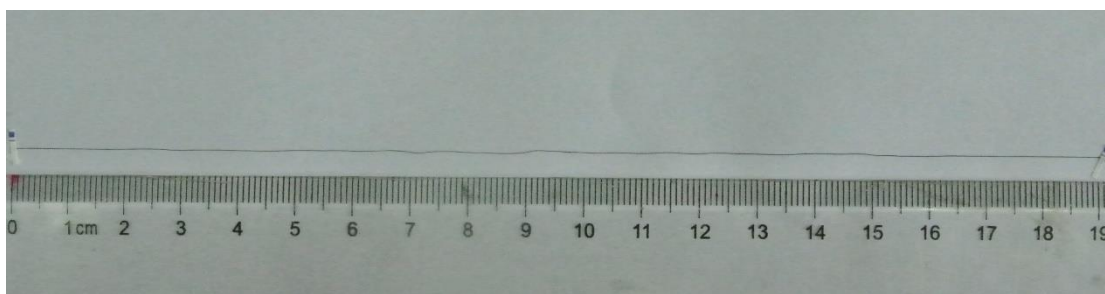


Figure S4. Photograph of a dry hybrid fiber with diameter of $\sim 70 \mu\text{m}$ and length of $\sim 20 \text{ cm}$.

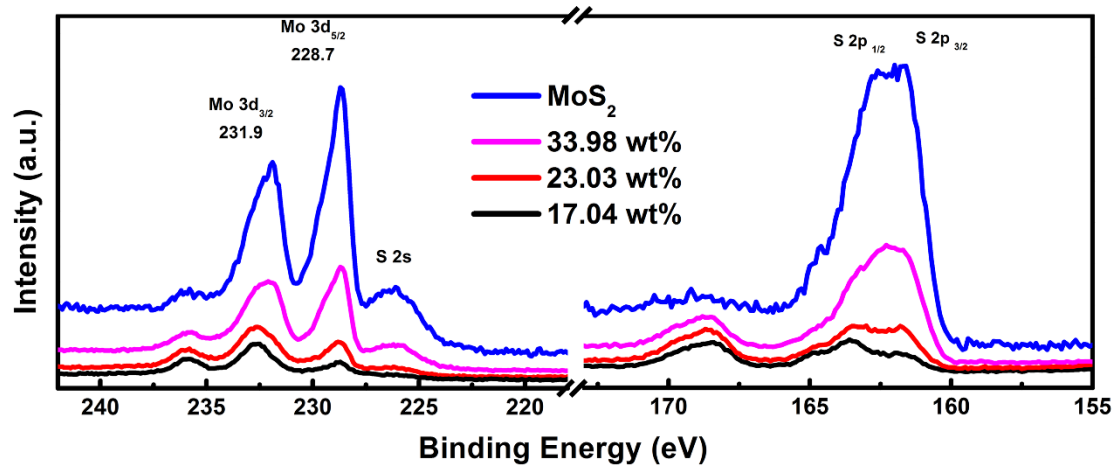


Figure S5. X-ray photoelectron spectroscopy spectra of graphene/MoS₂ hybrid fibers.

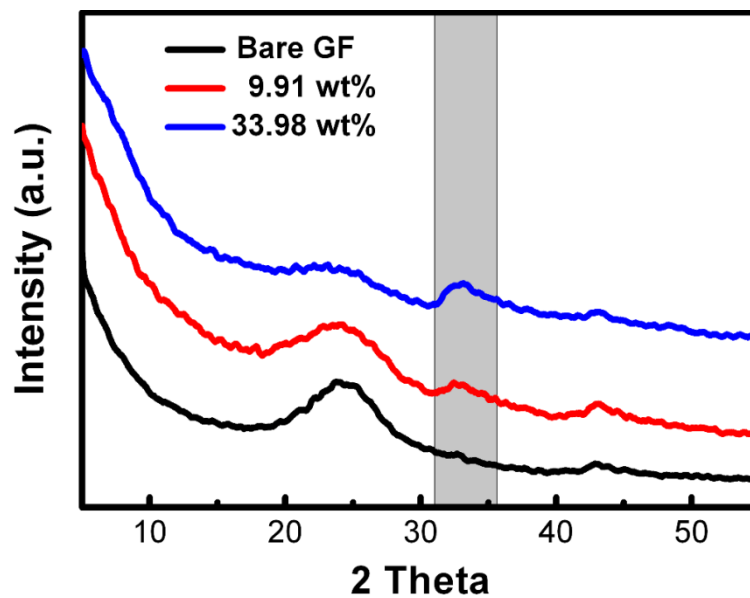


Figure S6. X-ray diffraction patterns of bare graphene and graphene/MoS₂ hybrid fibers with increasing MoS₂ contents.

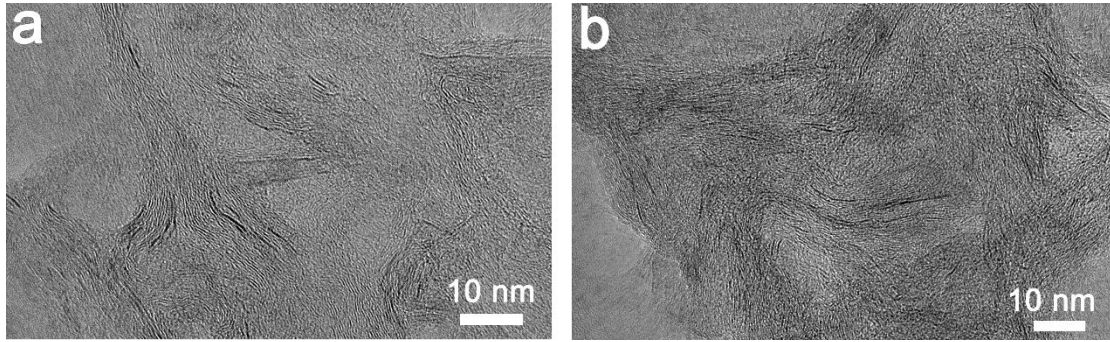


Figure S7. TEM images of the axial cross section of graphene/MoS₂ hybrid fibers with different MoS₂ content (**a**, 23.03 wt%; **b**, 33.98 wt%).

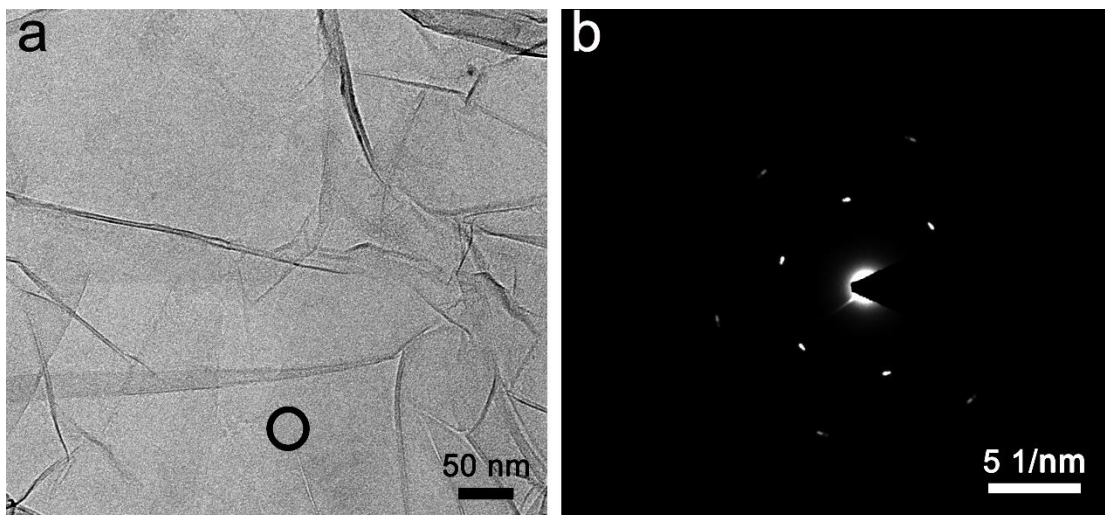


Figure S8. **a.** TEM image of reduced graphene oxide sheet. **b.** Selected area electron diffraction pattern of the circled region at **a.**

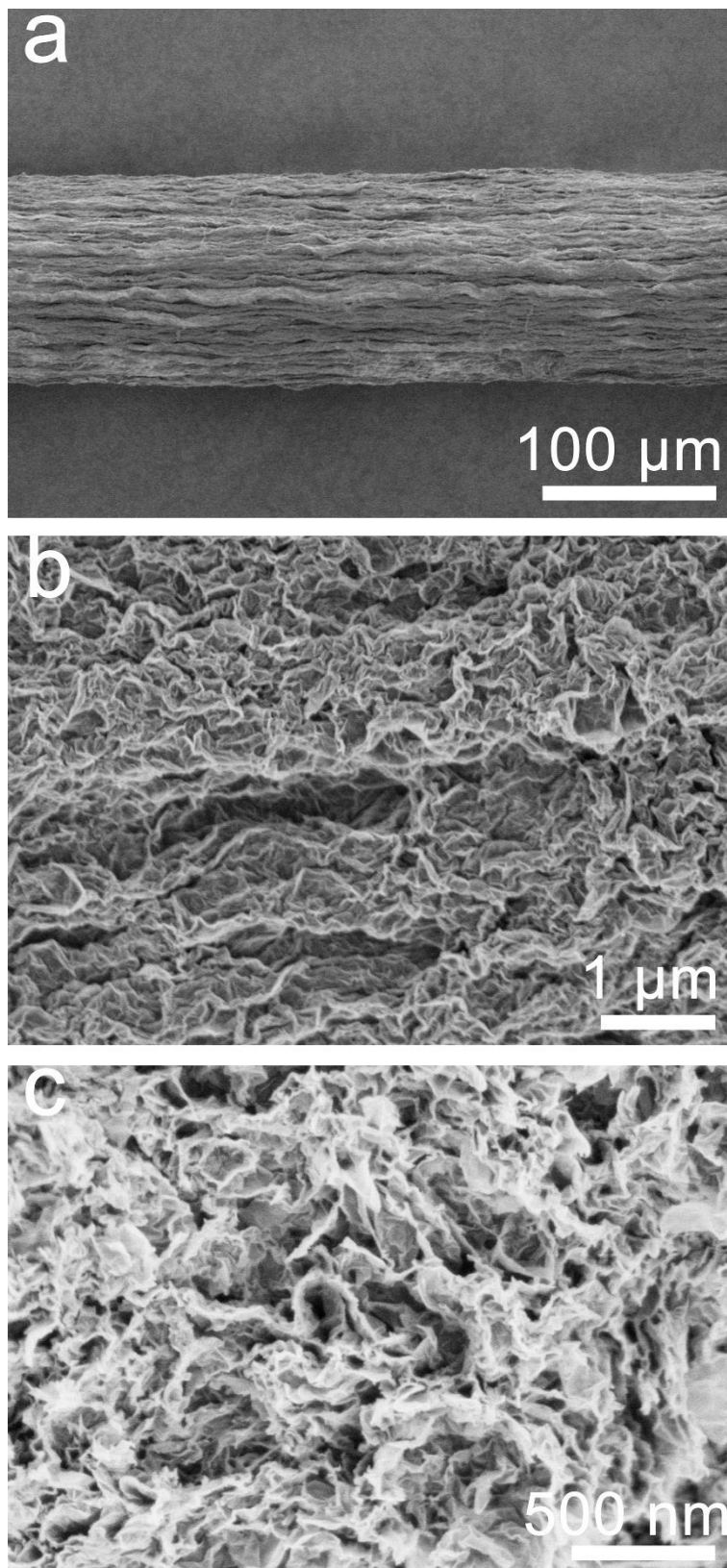


Figure S9. SEM images of a graphene/MoS₂ hybrid fiber (MoS₂ content of 2.06 wt%). **a** and **b**. Low and high magnifications by side view, respectively. **c**. High magnification by top view.

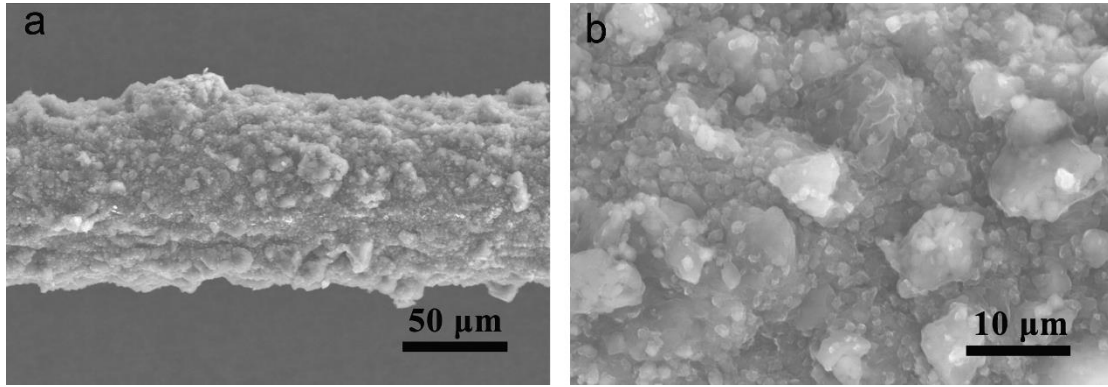


Figure S10. SEM images of a wet-spun graphene/MoS₂ hybrid fiber (MoS₂ content of 15 wt%) at low (a) and high (b) magnifications.

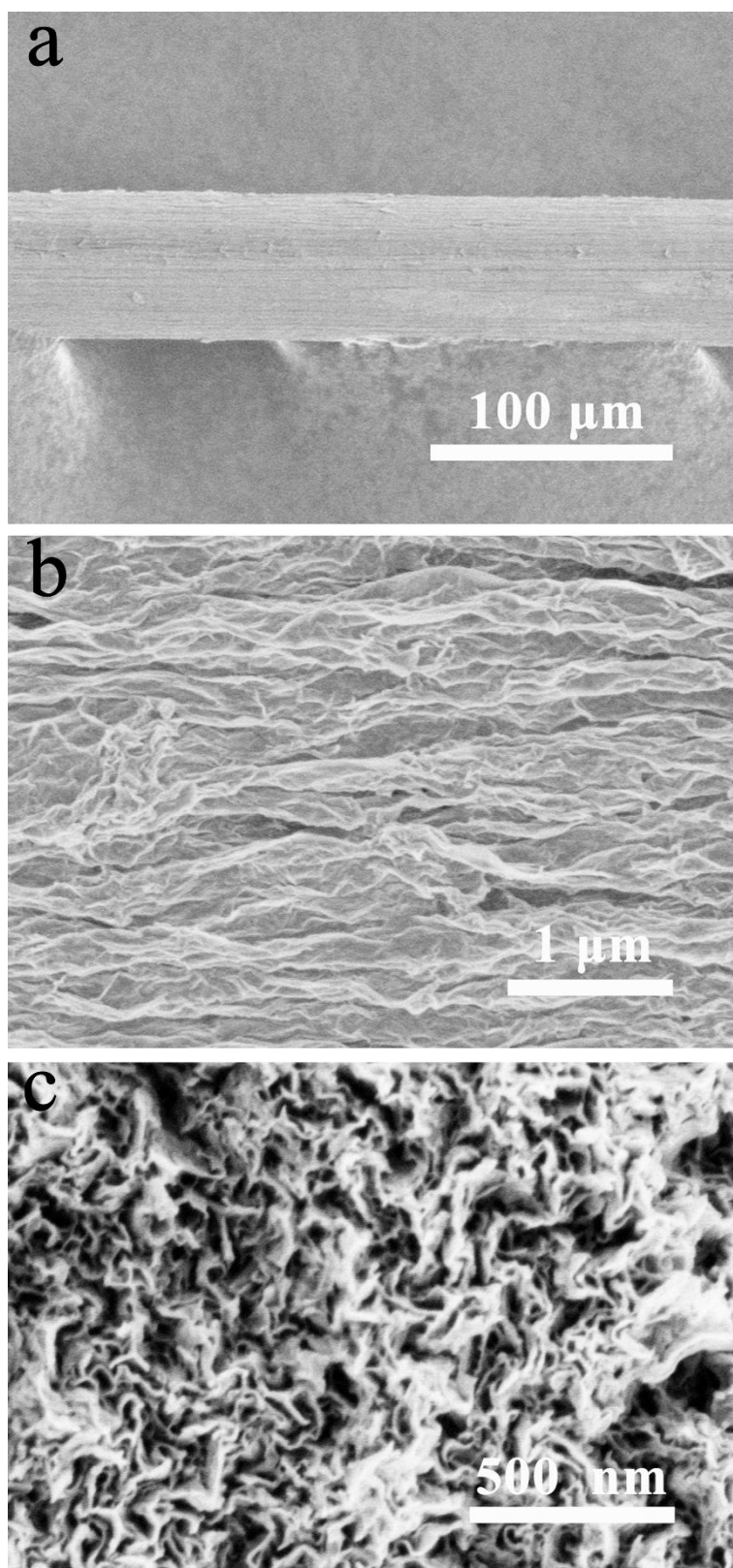


Figure S11. SEM images of a graphene/MoS₂ hybrid fiber (MoS₂ content of 23.03 wt%). **a** and **b**. Low and high magnifications by side view, respectively. **c**. High magnification by top view.

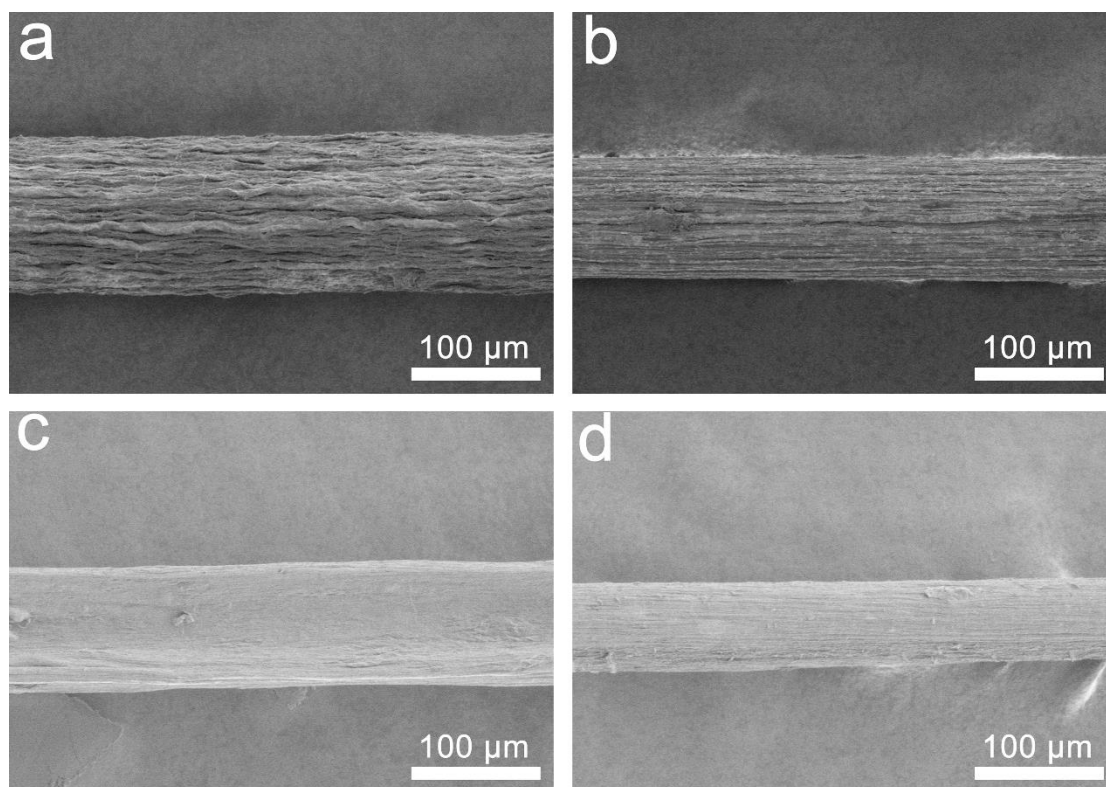


Figure S12. SEM images of graphene/MoS₂ hybrid fibers with increasing MoS₂ contents of 2.06 wt% (**a**), 9.91 wt% (**b**), 17.04 wt% (**c**) and 33.98 wt% (**d**). Shrinkage ratio is defined as the decreased diameter divided by the original diameter before drying, i.e., (wet diameter-dry diameter)/wet diameter.

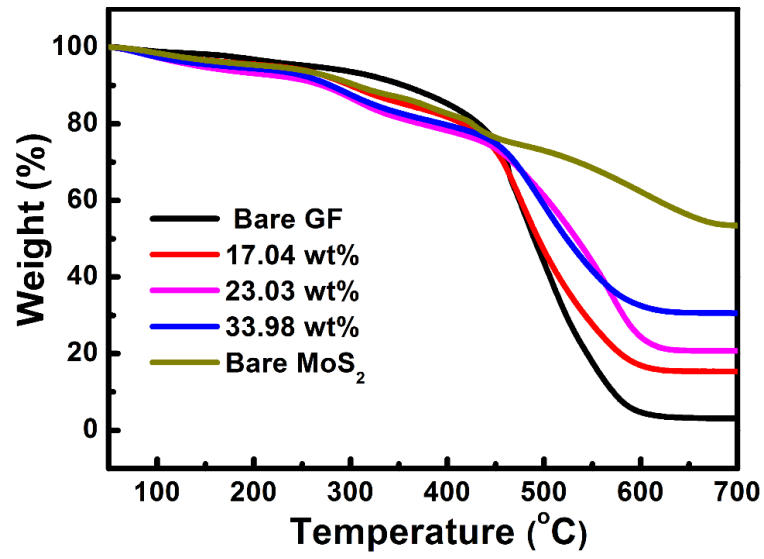


Figure S13. Thermo-gravimetric analysis of bare graphene and graphene/MoS₂ hybrid fibers with increasing MoS₂ contents.

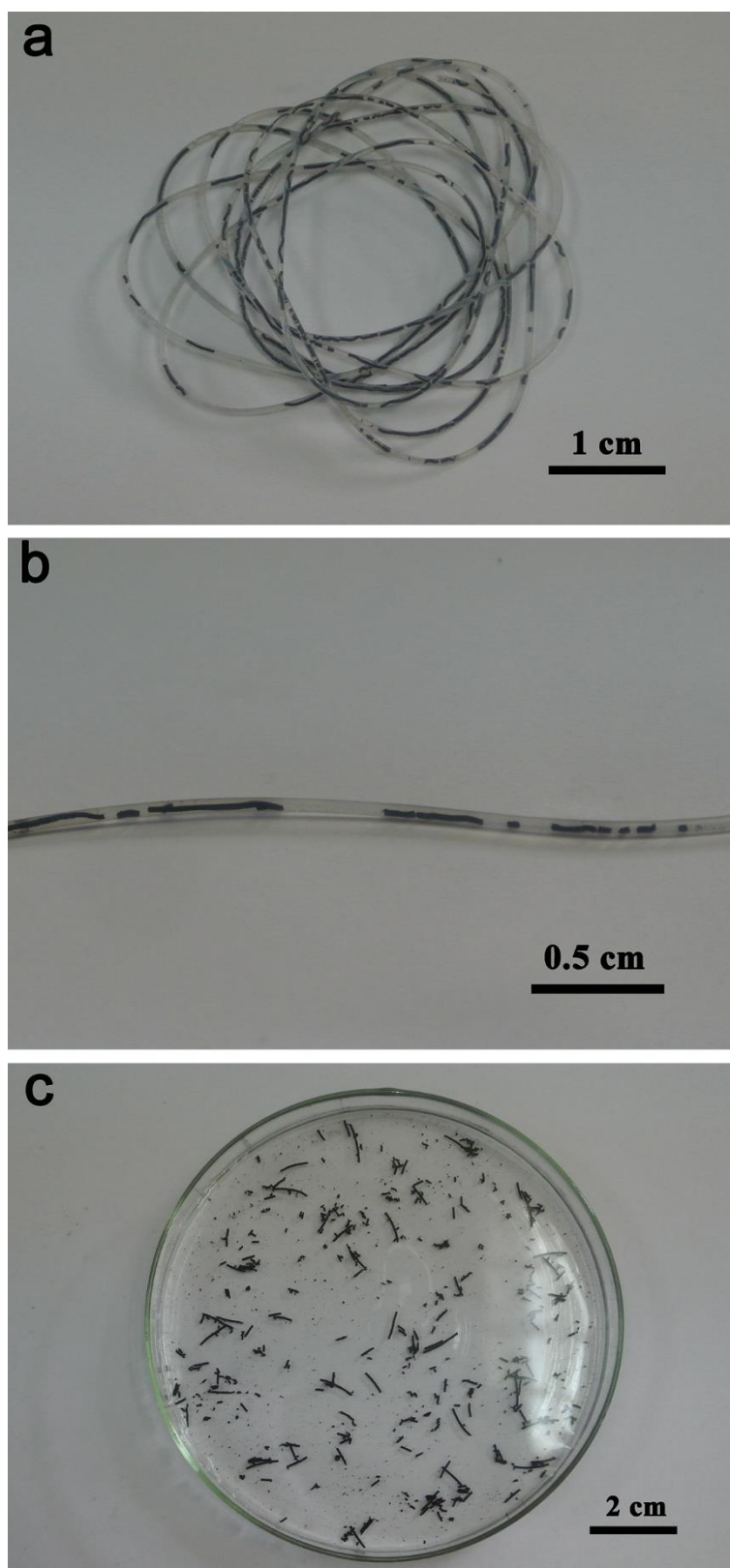


Figure S14. As-prepared graphene/MoS₂ hybrid fiber (MoS₂ content of 43.56 wt%). **a** and **b**. Photographs of an as-prepared graphene/MoS₂ hybrid fiber (MoS₂ content of 43.56 wt%) in PTFE tube after thermal treatment at low and high magnifications, respectively. **c**. Photograph of the broken graphene/MoS₂ hybrid fiber in water.

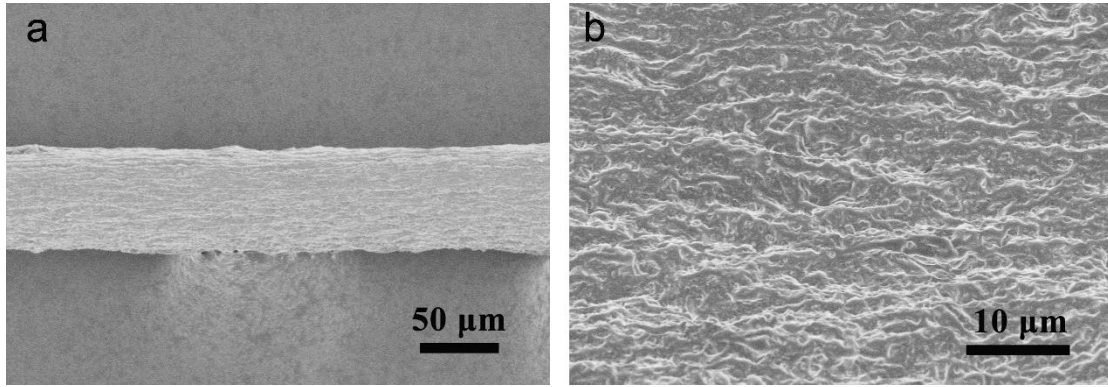


Figure S15. SEM images of a graphene/MoS₂ hybrid fiber (MoS₂ content of 43.56 wt%) at low (**a**) and high (**b**) magnifications, respectively.

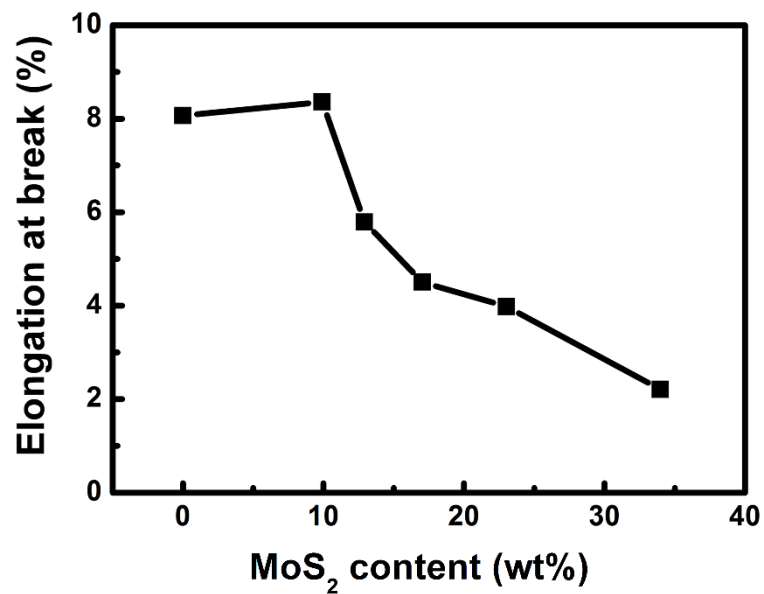


Figure S16. Dependence of breaking elongation on MoS₂ content at hybrid fibers.

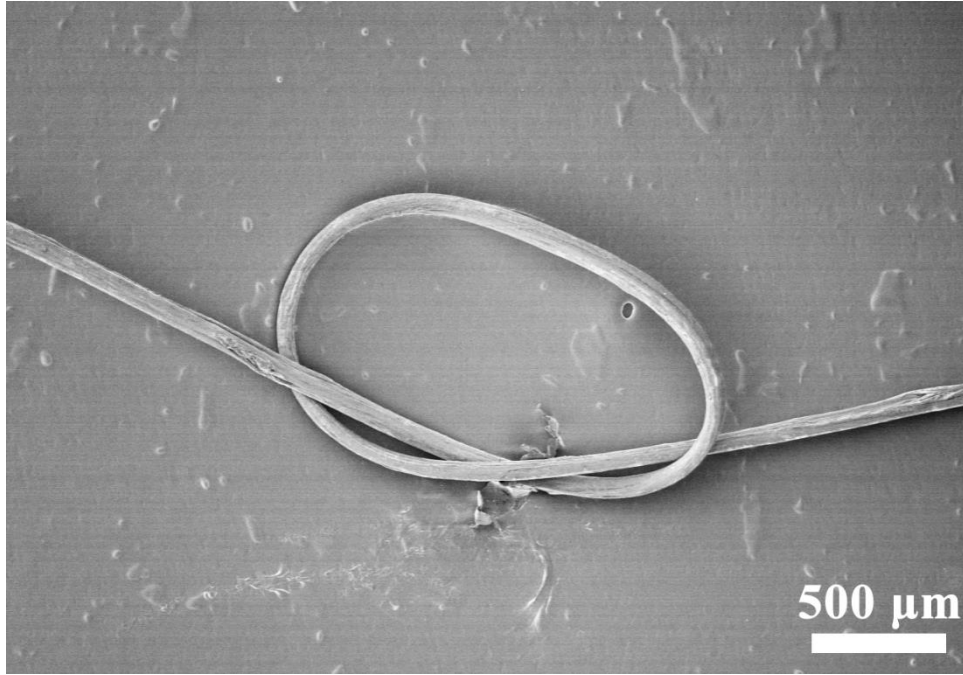


Figure S17. SEM image of a knotted hybrid fiber with MoS₂ content of 17.04 wt%.

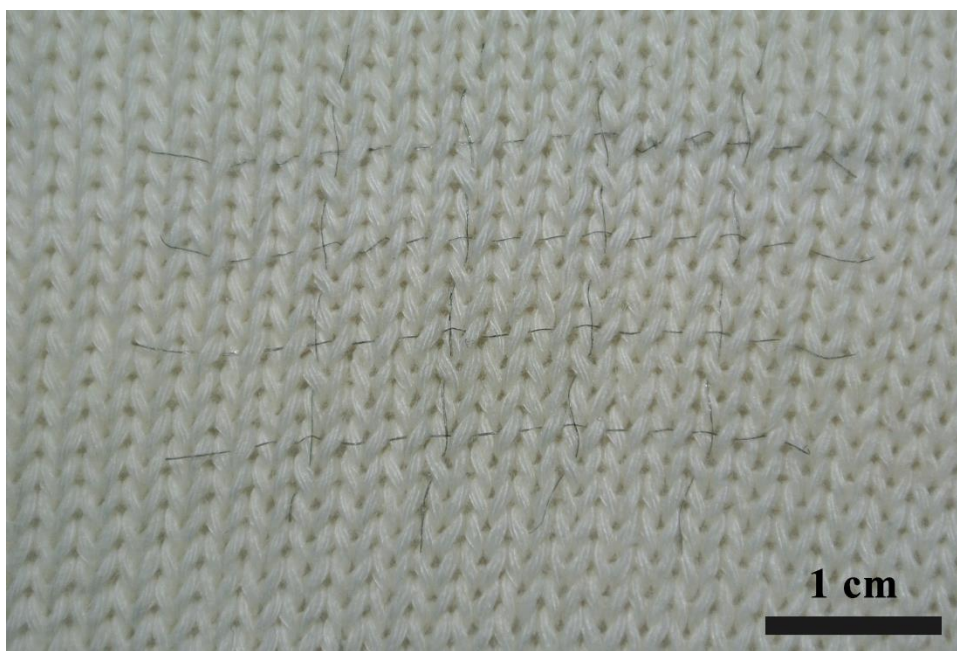


Figure S18. Photograph of a textile woven with graphene/MoS₂ hybrid fibers.

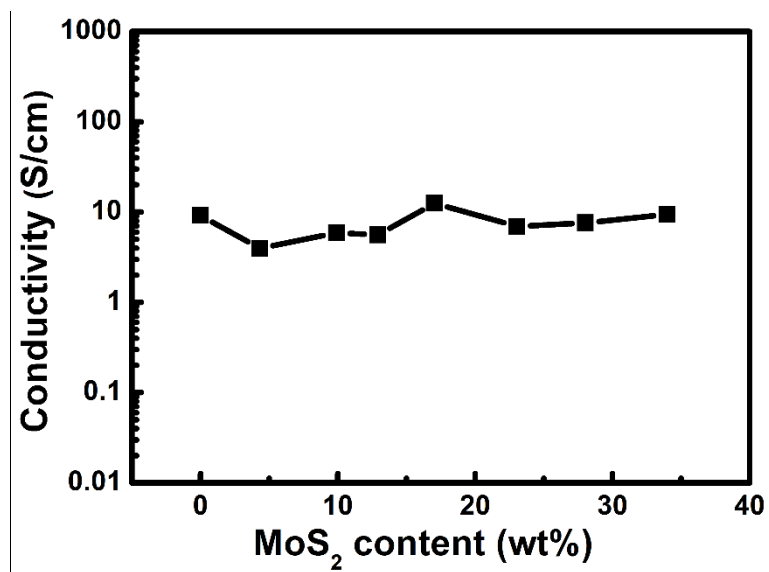


Figure S19. Dependence of electrical conductivity on MoS₂ content at the hybrid fiber.

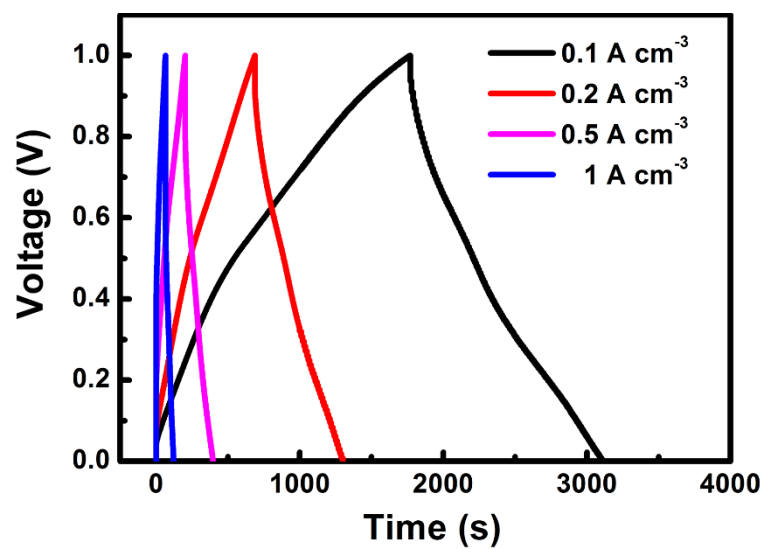


Figure S20. Galvanostatic charge-discharge curves of a supercapacitor fabricated from graphene/MoS₂ hybrid fibers (MoS₂ content of 23.03 wt%) at increasing current densities.

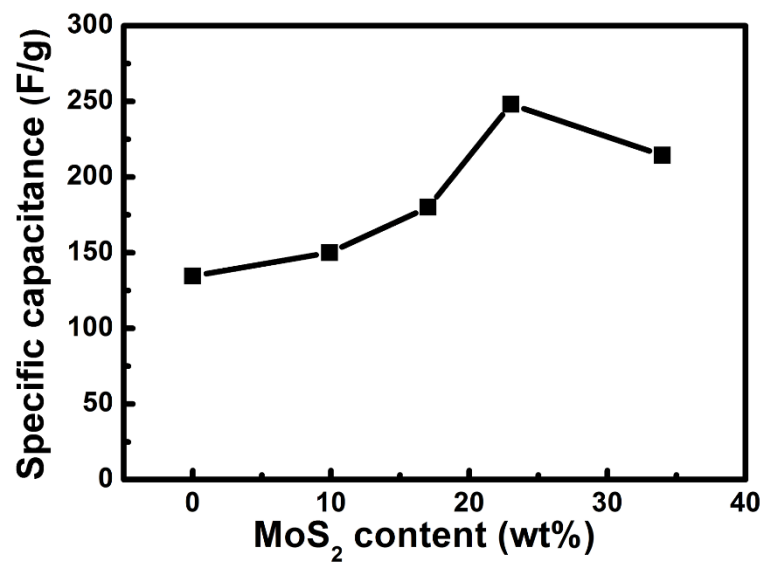


Figure S21. Dependence of mass specific capacitance on MoS₂ content in supercapacitor.

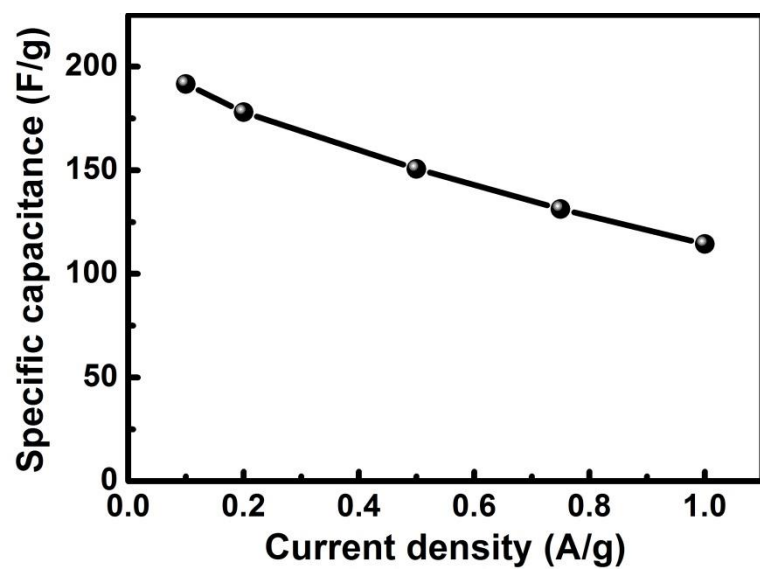


Figure S22. Mass specific capacitance of a supercapacitor derived from graphene/MoS₂ hybrid fibers (MoS₂ content of 33.98 wt%) at increasing current densities.

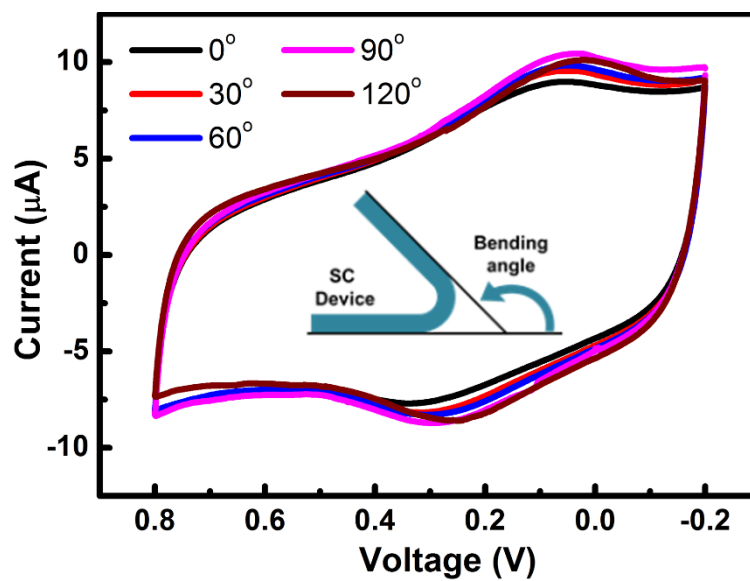


Figure S23. Cyclic voltammograms of a supercapacitor derived from the graphene/MoS₂ hybrid fiber (MoS₂ content of 23.03 wt%) before and after bending with increasing bending angles.

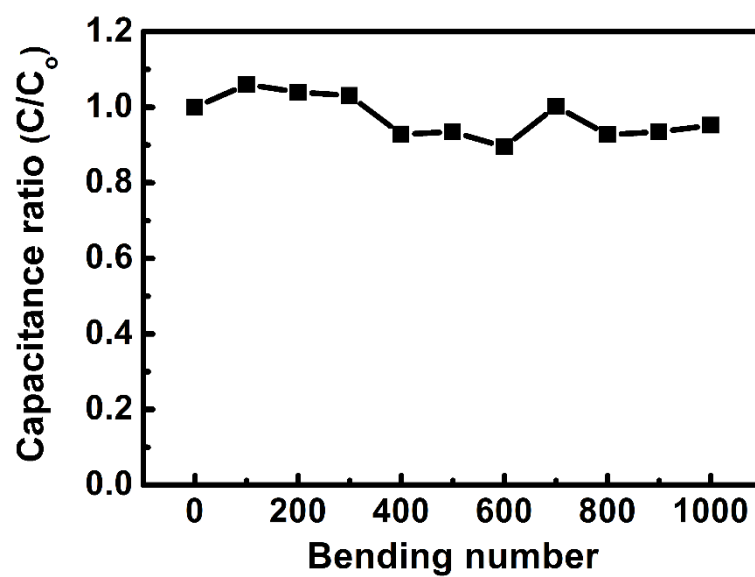


Figure S24. The cycling properties of a supercapacitor derived from the graphene/MoS₂ hybrid fiber (MoS₂ content of 23.03 wt%) with increasing bending number (Bending angle: 90°).